NEUTRINO PHYSICS: RECENT THEORETICAL DEVELOPMENTS*

Alexei Yu. Smirnov

International Centre for Theoretical Physics
Strada Costiera 11, 34014 Trieste, Italy
smirnov@ictp.trieste.it

and

Institute for Nuclear Research, RAS, Moscow, Russia

(Received August 6, 2008)

Some recent developments in theory and phenomenology of neutrino mass and mixing are described. These include new results in theory of neutrino propagation: neutrino oscillograms of the Earth and non-linear neutrino physics with applications to supernova neutrinos. Results of the bottom-up approach to understanding neutrino masses and mixing are summarized. Emergence of the "standard neutrino scenario" and searches for physics beyond this scenario are discussed.

PACS numbers: 14.60.Pq, 14.60.St

1. Introduction

1.1. 10 years after discovery

It took more than 70 years since Pauli's original idea (1930) that neutrino mass is of the order of the electron mass (or smaller) and the first Fermi's estimation (1934) that $m_\nu < 0.1 m_e$ to conclude that at least one neutrino mass is in the range

$$m = (0.04 - 0.20)\,\mathrm{eV}\,. \tag{1}$$

Behind this conclusion one finds marvelous work of several generations of theoreticians and experimentalists. The scale (1) is about $10^{-7} m_e$, $10^{-10} m_p$, $10^{-12} m_t$, and the latter provides strong evidence that we are touching something really new.

* Presented at the XXXVI International Meeting on Fundamental Physics, Baeza (Jaén), Spain, February 4–8, 2008.

About 50 years ago in the paper "Mesonium and antimesonium" [1] Pontecorvo has mentioned a possibility of neutrino oscillations which implied non-zero neutrino mass and mixing. Incidentally, in the same year 1957, discovery of the parity violation has been announced. This led to establishing the V–A theory of the weak interactions, and theory of two component massless neutrino which was dominating idea for almost 40 years. As we know for 10 years, the first line won.

This review has two parts. The first one is devoted to recent developments in theory of neutrino propagation which includes effects of passage of high energy neutrinos through the Earth and non-linear neutrino physics with applications to supernova (SN) neutrinos. The second part is towards the underlying physics, it covers the bottom-up approach in understanding neutrino mass and mixing; emergence of the "standard neutrino scenario", and exploration of physics beyond this scenario.

1.2. Neutrino mass and mixing

The *flavor* neutrinos, $\nu_f \equiv (\nu_e, \nu_\mu, \nu_\tau)$ are defined as the neutrinos that correspond to certain charge leptons: e, μ and τ. The correspondence is established by the weak interactions: ν_l and l ($l = e, \mu, \tau$) form the charged currents or doublets of the SU(2) symmetry group. Neutrinos, ν_1, ν_2, and ν_3, with definite masses m_1, m_2, m_3 are the eigenstates of mass matrix as well as the eigenstates of the total Hamiltonian in vacuum.

The *vacuum mixing* means that the flavor states do not coincide with the mass eigenstates. The flavor states are combinations of the mass eigenstates:

$$\nu_l = U_{li}\nu_i\,, \qquad l = e, \mu, \tau\,, \qquad i = 1, 2, 3\,, \tag{2}$$

where the mixing parameters U_{li} form the PMNS mixing matrix $U_{\rm PMNS}$ [1,2]. The mixing matrix can be conveniently parameterized as

$$U_{\rm PMNS} = V_{23}(\theta_{23}) I_{-\delta} V_{13}(\theta_{13}) I_\delta V_{12}(\theta_{12})\,, \tag{3}$$

where V_{ij} is the rotation matrix in the ij-plane, θ_{ij} is the corresponding angle and $I_\delta \equiv {\rm Diag}(1, 1, e^{i\delta})$ is the matrix of CP-violating phase.

Positive results on neutrino mass and mixing have been obtained from the solar neutrino experiments, KamLAND, atmospheric neutrino studies, MINOS, K2K [3]. A number of experiments provided important bounds: beta decay, CHOOZ, supernova SN1987A, Cosmology, double beta decay.

Two sets of results should be considered separately. (1) The double beta decay data of the Heidelberg–Moscow group [4] being interpreted as due to exchange of light Majorana neutrinos would imply the degenerate neutrino mass spectrum. This interpretation is, however, in conflict with the

cosmological bounds [5–7]. It is not excluded that the Heidelberg–Moscow result is dominantly due to some other mechanism of the lepton number violation. (2) MiniBooNE [8] excluding interpretation of the LSND excess [9] in terms of two neutrino oscillations (in the presence of sterile neutrinos), has created a new (low energy) anomaly. Being confirmed these results can be "seeds" of new physics which goes beyond the "standard" three-neutrino scenario.

The present determination of the neutrino oscillation parameters is essentially based on two effects of neutrino propagation driven by non-zero mass squared differences and mixing:

1. vacuum oscillations (both averaged and non-averaged) [1, 2, 10];
2. adiabatic conversion in medium with monotonously changing density — the MSW-effect [11, 12].

Another effect (at about 1σ level) — oscillations in matter — should also be taken into account in the analysis. It is relevant for the solar and atmospheric neutrinos passing through the Earth (see review [13]).

Information obtained from the oscillation experiments is encoded in the neutrino mass and flavor spectrum shown in figure 1. Unknown yet are *(i)* admixture of ν_e in ν_3, U_{e3}; *(ii)* type of mass spectrum: related to the value of the absolute mass scale, m_1; *(iii)* type of mass hierarchy (ordering); *(iv)* CP-violation phase δ.

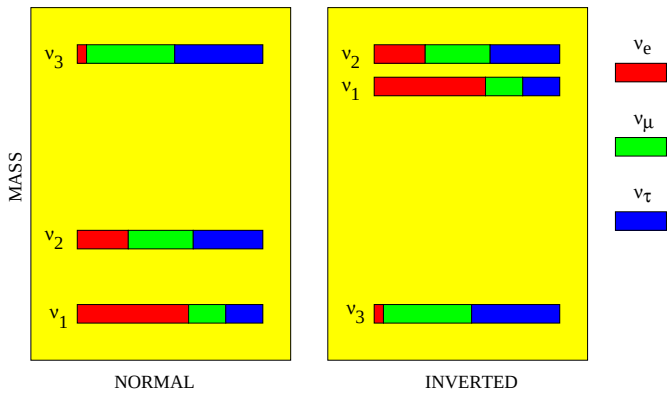

Fig. 1. Neutrino mass and flavor spectra for the normal (left) and inverted (right) mass hierarchies. The distribution of flavors is shown by shaded (colored) parts of boxes in the mass eigenstates; we take $\sin^2\theta_{13} = 0.05$.

2. To the theory of neutrino conversion

2.1. Describing neutrino evolution

The master equation which describes flavor neutrino propagation in the transparent media is

$$i\frac{d\nu_f}{dt} \approx H\nu_f\,, \tag{4}$$

where H is the Hamiltonian:

$$H = \frac{MM^\dagger}{2E} + V\,, \qquad V = \mathrm{Diag}(V_e, 0, 0)\,. \tag{5}$$

Here $MM^\dagger \equiv U_{\mathrm{PMNS}} M^2_{\mathrm{Diag}} U^\dagger_{\mathrm{PMNS}}$ is the mass matrix squared in the flavor basis and $V_e \equiv \sqrt{2} G_{\mathrm{F}} n_e$ is the matter potential due to the charged current scattering of ν_e on electrons ($\nu_e e \to \nu_e e$) [11], G_{F} is the Fermi coupling constant and n_e is the number density of electrons.

The potential (refraction index) determines the *refraction length*:

$$l_0 \equiv \frac{2\pi}{V_e} = \frac{\sqrt{2}\pi}{G_{\mathrm{F}} n_e} \tag{6}$$

— the distance over which an additional "matter" phase equals 2π. The energy-quantity relevant for dynamics of neutrino propagation in vacuum is the *frequency*

$$\omega \equiv \frac{\Delta m^2}{2E}\,. \tag{7}$$

The dynamics of conversion is determined by the interplay of V_e and ω.

It is convenient to describe the flavor evolution of neutrinos (especially in the cases of interest here) in terms of the neutrino *polarization vectors* (or density matrix). Let us consider for simplicity the two flavor system $\psi = (\nu_e, \tilde{\nu}_3)$, where $\tilde{\nu}_3 \equiv (\nu_\mu + \nu_\tau)/\sqrt{2}$. The neutrino polarization vector with frequency ω is defined as

$$\boldsymbol{P}_\omega \equiv \psi^\dagger_\omega \frac{\sigma}{2} \psi_\omega\,, \tag{8}$$

where σ are the Pauli matrices. Differentiating $\boldsymbol{P}_\omega$ and using equation of motion for the wave functions (4) we obtain

$$\partial_t \boldsymbol{P}_\omega = (\omega \boldsymbol{B} + \lambda \boldsymbol{L}) \times \boldsymbol{P}_\omega\,, \tag{9}$$

where $\boldsymbol{B} \equiv (\sin 2\theta, 0, \cos 2\theta)$ is the mass direction and θ is the vacuum mixing angle. (For the inverted mass hierarchy $\theta \to \pi/2 - \theta$.) The unit vector $\boldsymbol{L} = (0, 0, 1)$ is the flavor direction, so that $\boldsymbol{B} \cdot \boldsymbol{L} = \cos 2\theta$. Here

$\lambda = V_e$ is the usual matter potential. (For antineutrinos $\omega \to -\omega$.) The Eq. (9) coincides with the equation for spin of the electron in the magnetic field given by the vector $\omega \boldsymbol{B} + \lambda \boldsymbol{L}$. Graphic representation is based on this analogy.

2.2. Conditions for maximal flavor transformations

Oscillation (transition) probability in vacuum or in matter with constant density reads

$$P(\nu_e \to \nu_x) = \sin^2 2\theta_{\rm m} \sin^2 \phi \,, \tag{10}$$

where $\theta_{\rm m}$ is the mixing angle in matter, and $\phi \equiv \pi L/l_{\rm m}$ is the half-phase. The oscillation length equals $l_{\rm m} = 2\pi/(H_2 - H_1)$, where H_i are the eigenvalues of neutrinos in matter. The amplitude (depth) of oscillations is given by $\sin^2 2\theta_{\rm m}$ and $\sin^2 \phi(E, L)$ is the oscillatory factor.

The maximal transition probability, $P = 1$, implies that

1. $\sin^2 2\theta_{\rm m} = 1$ — the amplitude condition,

2. $\phi = \pi/2 + \pi k$ — the phase condition.

Generalizations of these conditions to the case of several layers with varying density play a crucial role in understanding oscillation effects.

In matter with constant density the amplitude condition is nothing but the MSW resonance condition: $\sin^2 2\theta_{\rm m} = 1$ or $l_\nu = l_0 \cos 2\theta$ (oscillation length in vacuum equals approximately the refraction length for small mixing, or the frequency equals potential). The phase condition is determined by dependence of the oscillation length on energy. At low energies (vacuum dominated regime):

$$l_{\rm m} \approx l_\nu = \frac{4\pi E}{\Delta m^2} \,. \tag{11}$$

The oscillation length increases and reaches maximum (for small θ) at $l_\nu = l_0/\cos 2\theta$ — slightly above the resonance. At further increase of energy, it approaches the refraction length: $l_{\rm m} \approx l_0$ and the dependence on energy disappears.

The resonance enhancement of oscillations [12] occurs when neutrino flux propagates through the layer with constant or weakly varying density (the situation relevant for neutrinos passing through the mantle of the Earth).

Parametric enhancement of oscillations is associated to certain conditions for the phases [14]. This is another way of getting strong transitions. No large vacuum mixing and no matter enhancement of mixing or resonance conversion are required. The amplitude condition for the castle wall profile

consisting of alternative layers with two different densities and lengths (relevant for neutrino oscillations inside the Earth) is reduced to the parametric resonance condition [15]:

$$\sin\phi_1 \cos\phi_2 \cos 2\theta_{1m} + \sin\phi_2 \cos\phi_1 \cos 2\theta_{2m} = 0\,, \tag{12}$$

where subscripts 1 and 2 denote the layers (see also [16]). One simple realization of this condition which does not depend on mixing angles is

$$\phi_1 = \frac{\pi}{2} + \pi k\,, \qquad \phi_2 = \frac{\pi}{2} + \pi n\,. \tag{13}$$

3. Passing through the Earth

Detailed consideration of the neutrino oscillations in the matter of the Earth has important applications to the atmospheric neutrinos, accelerator neutrinos and neutrinos of cosmic origins. The Earth density profile can be considered as consisting out of several layers with slowly changing density inside each and sharp change of the density at the borders. The most important structures being the core and the mantle, and factor of 2 density jump between them. So, neutrino oscillations in the Earth are oscillations in multi-layer medium with slowly changing density in the individual layer.

A comprehensive description of effects of this propagation can be given in terms of the neutrino oscillograms of the Earth — lines of equal probabilities (or certain combinations of probabilities) in the nadir angle, Θ_ν, — neutrino energy plain. In Fig. 2 we show the oscillograms for the total disappearance probability of electron neutrinos (and antineutrinos), $1 - P_{ee}$, where P_{ee} is the survival probability. In a sense, the oscillograms are the Earth portraits in the neutrino light or the neutrino images of the Earth.

3.1. Structure of oscillograms

The structure of oscillograms can be well understood using generalizations of the amplitude and phase conditions considered in Sec. 2.2 to the non-constant density case.

There are three steps in this generalization [17]:

1. take the conditions for constant density;
2. write them in terms of elements of the evolution matrix defined as

$$S = Te^{-i\int_0^x dy H(y)}\,, \tag{14}$$

3. apply the obtained conditions to the case of varying density.

It turns out that this generalization not only reproduces the original conditions but also leads to new realizations which explain other features of oscillograms such as local maxima, minima and saddle points. Thus, the generalization has more physics content.

The Earth is unique and the structures of oscillograms seen in Fig. 2 are well defined and unique. The main features of the oscillograms in the resonance channel (upper panels) can be listed in the following way:

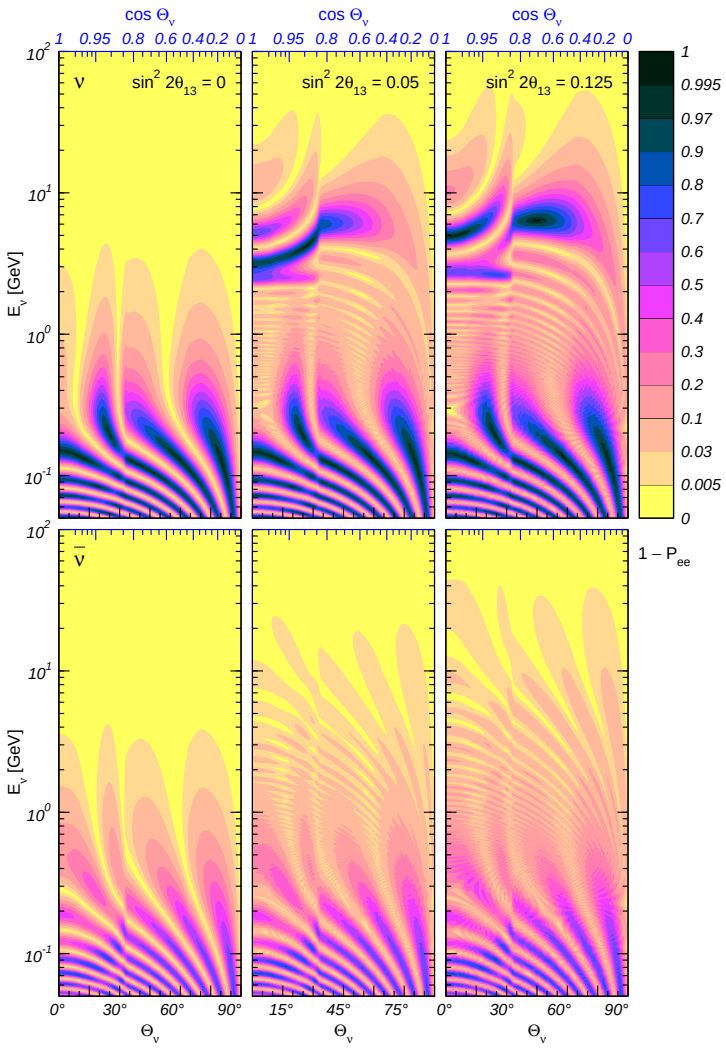

Fig. 2. Neutrino oscillograms in the 3ν-mixing case. Shown are the contours of constant probability $1 - P_{ee}$ (upper panels) and $1 - P_{\bar{e}\bar{e}}$ (lower panels) for $\Delta m^2_{21} = 8 \times 10^{-5}\,\mathrm{eV}^2$, $\tan^2\theta_{12} = 0.45$ and different values of θ_{13}. From [18].

Resonance structures due to the 1–2 mixing and mass split at low energies ($E < 1\,\mathrm{GeV}$) include:

1. The three (and only three) MSW peaks with maximal transition, $P_{ee} = 0$, in the mantle domain ($\Theta_\nu > 33^\circ$) at $E = (0.12\text{–}0.15)\,\mathrm{GeV}$. These peaks differ by values of the total half-phase acquired by neutrinos: $\pi/2$, $3\pi/2$, $5\pi/2$ from the outer peak to the inner one.
2. The parametric peak at $E = 0.2\,\mathrm{GeV}$ and $\Theta_\nu = 20^\circ$ (in the core domain) which corresponds to approximate realization of conditions (13). The lower energy structures, although can be interpreted as due to the parametric resonance, have small effect of interplay of the core and mantle oscillations. Here we have the resonance enhancement pattern. If 1–3 mixing is non-zero the resonance structure appears at $E > 2\,\mathrm{GeV}$. It includes:
3. One and only one resonance MSW peak at $E \sim 6\,\mathrm{GeV}$. This peak has maximal height, $P_{ee} = 0$, if $\sin^2 2\theta_{13} > 0.06$.
4. One MSW resonance peak in the core (for core crossing trajectories) at $E \sim 2.5\,\mathrm{GeV}$. Here the half-phases in the mantle layers are $\phi = \pi$ and therefore the oscillations in mantle does not contribute to the transition effect.
5. Three parametric resonance ridges in the range $E \sim (3\text{–}20)\,\mathrm{GeV}$. The ridges differ by the phase acquired in the core.

The 1–3 pattern emerges at $\sin^2 2\theta_{13} \sim 0.01$ at zero nadir angle and then with increase of θ_{13} moves along fixed lines of flow to large Θ_ν.

For the non-zero 1–3 mixing one observes also an interference of the 1–2 and 1–3 oscillation patterns: the interference of the modes with 1–2 and 1–3 mass splits and mixings. In other channels the interference depends on the CP-phase and manifests the CP violation effects.

3.2. Interference. CP violation

Let us consider the CP violation in the $\nu_\mu \to \nu_e$ channel. The transition probability can be written as

$$\begin{aligned} P_{\mu e} &= |\cos\theta_{23} A_{e\tilde{2}} + \sin\theta_{23} e^{-i\delta} A_{e\tilde{3}}|^2 \\ &= \cos^2\theta_{23}|A_{e\tilde{2}}|^2 + \sin^2\theta_{23}|A_{e\tilde{3}}|^2 + \sin 2\theta_{23}|A_{e\tilde{2}}A_{e\tilde{3}}|\cos(\phi - \delta)\,, \quad (15) \end{aligned}$$

where $A_{e\tilde{2}}$ is the amplitude of $\nu_e \to \nu_{\tilde{2}} \equiv (\nu_\mu - \nu_\tau)/\sqrt{2}$ transition, and $A_{e\tilde{3}}$ is the amplitude of $\nu_e \to \nu_{\tilde{3}} \equiv (\nu_\mu + \nu_\tau)/\sqrt{2}$ transition. Notice that these amplitudes do not depend on θ_{23} and δ, and in Eq. (15) the dependence of $P_{\mu e}$ on these parameters is explicit. In the last equality,

$$\phi \equiv \mathrm{Arg}(A^*_{e\tilde{2}} A_{e\tilde{3}}) \quad (16)$$

is the interference phase.

To assess the δ-dependent interference terms, one can consider the difference of the oscillation probabilities for two different values of the CP-phase:

$$\Delta P^{\rm CP}_{\mu e}(\delta) \equiv P_{\mu e}(\delta) - P_{\mu e}(\delta_0)\,. \tag{17}$$

The condition $\Delta P^{\rm CP}_{\mu e} = 0$ is equivalent to

$$|A_{e\tilde{2}} A_{e\tilde{3}}| \cos(\phi - \delta) = |A_{e\tilde{2}} A_{e\tilde{3}}| \cos(\phi - \delta_0)\,. \tag{18}$$

The same equality holds for the $\nu_e - \nu_\tau$ channel. This equality is satisfied if at least one of the following three conditions is fulfilled

$$\text{(A)} \qquad A_{e\tilde{2}}(E_\nu, \Theta_\nu) \;=\; 0\,, \tag{19a}$$

$$\text{(B)} \qquad A_{e\tilde{3}}(E_\nu, \Theta_\nu) \;=\; 0\,, \tag{19b}$$

$$\text{(C)} \qquad \phi(E_\nu, \Theta_\nu) \;=\; (\delta + \delta_0)/2 + \pi l\,. \tag{19c}$$

Under conditions (A) and (B) the equality (18) is satisfied identically for all values of δ and the transition probability does not depend on CP-phase.

Due to smallness of 1–3 mixing and strong hierarchy of mass squared differences one finds [18]

$$A_{e\tilde{2}} \approx A_{\rm S}(\Delta m^2_{21}, \theta_{12})\,, \qquad A_{e\tilde{3}} \approx A_{\rm S}(\Delta m^2_{31}, \theta_{13})\,, \tag{20}$$

that is, in the first approximation $A_{e\tilde{2}}$ depends only on the "solar" oscillation parameters with small corrections from 1–3 mixing, whereas $A_{e\tilde{3}}$ depends only on the "atmospheric" parameters with small corrections due to 1–2 mass splitting. (Strictly speaking for $A_{e\tilde{2}}$ this is valid below the 1–3 resonance.) We call equalities (20) the *factorization approximation*.

In the factorization approximation the conditions in (A), (B) and (C) define three sets of lines in the oscillograms (see Fig. 3), which play crucial role in understanding effects of CP violation. Along the lines determined by (A) and (B) the probabilities $P_{\mu e}$ as well as $P_{e\mu}$ $P_{\tau e}$ and $P_{e\tau}$ do not depend on the CP-phase. (The other probabilities only weakly depend on the phase along these lines.) The lines shown in Fig. 3 were calculated in the factorization approximation, without assuming constant-density matter.

At $A_{\rm S}(E_\nu, \Theta_\nu) = 0$ (in factorization approximation) the "solar" contribution to the amplitudes of the $\nu_\mu \leftrightarrow \nu_e$ and $\nu_\tau \leftrightarrow \nu_e$ transitions vanishes. In Fig. 3 this condition determines nearly vertical lines at the values of the nadir angle $\Theta_\nu \approx 54^\circ$, 30° and 12° [18–20]. This feature can be understood using the constant density approximation [20], where the condition $A_{\rm S} = 0$ is fulfilled if

$$\sin \phi_{\rm S}(E_\nu, \Theta_\nu) = 0\,, \tag{21}$$

or $\phi_{\rm S}(E_\nu, \Theta_\nu) = \pi k$. As we mentioned in Sec. 2.2, at energies much higher than the solar resonance energy, $l_{\rm m} \approx l_0$, and the condition (21) becomes

$$L(\Theta_\nu) \simeq \frac{2\pi n}{V_e}\,. \tag{22}$$

It is energy independent.

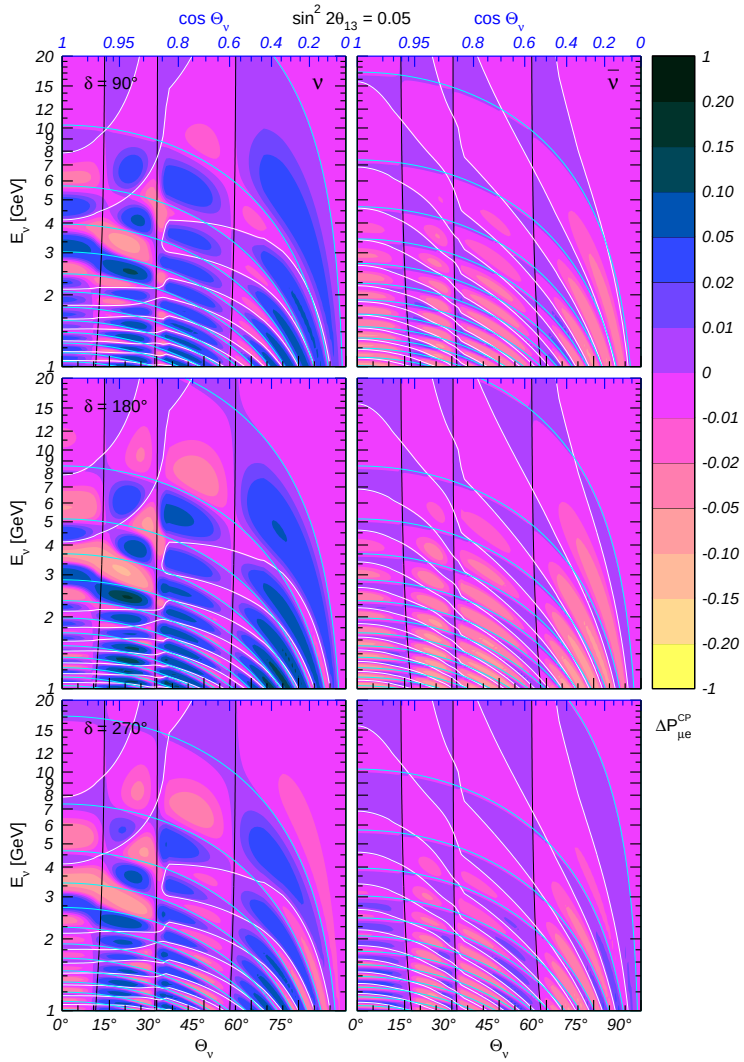

Fig. 3. Oscillograms for the difference of probabilities $\Delta P^{\rm CP}_{\mu e}(\delta) = P_{\mu e}(\delta) - P_{\mu e}(\delta_0)$ with $\delta_0 = 0°$. Shown are the solar (black/blue), atmospheric (white) and interference phase condition (gray/cyan) curves.

When the condition $A_{\rm A}(E_\nu, \Theta_\nu) = 0$ is satisfied, the "atmospheric" contribution to the transition amplitude vanishes. Along the atmospheric "magic" lines there are no effects of CP-phase on the oscillations involving ν_e or $\bar{\nu}_e$. For energies which are not too close to the 1–3 MSW resonance, the condition $A_A = 0$ in the constant density approximation reduces to

$$E_\nu \simeq \frac{\Delta m^2_{31} L(\Theta_\nu)}{|4\pi k \pm 2VL(\Theta_\nu)|} \,. \tag{23}$$

In the energy range between the two resonances one obtains $\phi \approx -\phi^m_{31} \approx \phi_{31}$ and the interference phase condition does not depend on matter density

$$E_\nu = \frac{\Delta m^2_{31} L(\Theta_\nu)}{4\pi l - 2(\delta + \delta_0)} \,. \tag{24}$$

The solar (nearly vertical) and atmospheric (bent) lines divide the oscillograms into a set of domains (CP violation domains), which are in turn divided by the grid of the interference phase lines into sub-domains (see Fig. 3). CP violation is zero along the lines. The CP violation effects are maximal in the centers of the domains and they have opposite signs in the neighboring domains. With change of δ the solar and atmospheric lines do not change, whereas the interference phase lines monotonously move changing configuration of sub-domains. One can show that for the $\mu\mu-$ and $\mu\tau-$ channels the dependencies of the interference terms on ϕ and δ factorize, *e.g.* $\mathrm{Int}[P_{\mu\mu}] = \sin 2\theta_{23} |A_{e\tilde{2}} A_{e\tilde{3}}| \cos\phi \cos\delta$, and therefore borders of domains do not change with δ. This behavior of oscillograms allows one to elaborate criteria for measurements of the CP-phase.

3.3. Measuring oscillograms

Measurements of oscillograms open a possibility to *(i)* study various oscillation effects, *e.g.* parametric enhancement of oscillations; *(ii)* determine unknown neutrino parameters: 1–3 mixing, mass hierarchy and CP-phase; *(iii)* search for non-standard physics; *(iv)* perform tomography of the Earth with spatial resolution $> 100\,$km.

What are possible tools for these measurements?

1. Operating and expected accelerator experiments (superbeams, beta beams, muon factories) cover the energy range (0.5–30) GeV and several baselines at $\cos\Theta_\nu < 0.3$, that is, the peripherical regions of oscillograms with poor structure. This is the origin of various degeneracies: the same modification of the oscillatory pattern can be produced varying different parameters (*e.g.* θ_{13} and δ).

2. Atmospheric neutrinos cover huge ranges of energies, $E = (0.1\text{–}10^4)$ GeV and base-lines, $(10\text{–}10^4)$ km. (The latter corresponds to whole range of the nadir angles.) The problem here is low statistics (especially at high energies) and uncertainties in the original neutrino fluxes. The present large-scale underground and under-ice detectors (AMANDA, IceCube, Antares) have high energy thresholds ($E > (50\text{–}100)$ GeV) thus missing the most interesting and structured region of oscillograms at $E = (2\text{–}10)$ GeV.

Both problems can be resolved with multi-Megaton detectors of the TITAND type with energy threshold below (1–2) GeV [21]: high statistics will allow one to measure oscillograms in wide $E - \Theta_\nu$ range and determine both unknown neutrino parameters and original fluxes (uncertainties can be parameterized by few quantities) simultaneously.

4. Non-linear neutrino physics

Detection of neutrino bursts from a Galactic supernova can substantially contribute to determination of the neutrino parameters (1–3 mixing, mass hierarchy) and reconstruction of neutrino mass spectrum [22–25]. This determination is based on the effects of MSW conversions inside the star as well as oscillations in the matter of the Earth [22].

Recently it has been realized that usual picture of the MSW transitions in the envelope of star can be substantially modified by the collective effects related to neutrino self-interactions ($\nu\nu$-scattering) in central parts of a star [26–37]. This field is still in explorative phase.

4.1. Flavor exchange. Evolution equations

Non-trivial collective effects are related to phenomenon of coherent *flavor exchange* which can be understood in the following way [26, 30]. Consider scattering of the probe neutrino, *e.g.* ν_e, on the background neutrinos, ν_b. The $\nu\nu$-scattering can proceed due to momentum exchange Z^0-boson exchange in the t- and u- channels. In the first case the coherence requires scattering onto zero angle (zero momentum transfer):

$$|e\rangle + |b, b, ...\, b\rangle \to |e\rangle + |b, b, ...\, b\rangle\,. \tag{25}$$

ν_b does not change momentum and therefore scattering on all components of the background is coherent. This scattering is flavor diagonal and the same for all neutrino species. Therefore, it does not contribute to the flavor evolution. In the second case the original electron neutrino exchanges momentum with one of neutrinos in the background: ν_e goes into background

whereas one of neutrinos from background picks up momentum of ν_e. So, the process can be considered as the *flavor exchange* between the probe particle and background:

$$|e\rangle + |b, b, ...\, b\rangle \to |b\rangle + |e, b, ...\, b\rangle\,. \tag{26}$$

Here ν_e is exchanged with the first component ν_b of background. Similarly one should write exchange with all other components of the background: $|b\rangle + |b, e, ...\, b\rangle$, *etc.* Scattering on different components of the background will be coherent if ν_b is not orthogonal to ν_e: $|b\rangle = \psi_{eb}|e\rangle + \psi_{xb}|x\rangle$, where $|\nu_x\rangle$ is orthogonal to $|\nu_e\rangle$. Indeed, since $|b\rangle$ contains component of $|x\rangle$ and $|e\rangle$ contains $|b\rangle$, the process (27) will have a sub-channel

$$|e\rangle + |b, b, ...\, b\rangle \to |x\rangle + |b, b, ...\, b\rangle \tag{27}$$

with the amplitude of probability $\psi_{be}\psi_{xb}$. In this case the background does not change and therefore scattering on all components of background is coherent. Apart from this flavor off-diagonal transition there are also flavor diagonal transitions. As a result, the $\nu\nu$- scattering leads to additional term of the Hamiltonian: non-diagonal matrix which is proportional to the neutrino density and projections of the background state onto involved flavor states: $H_{\nu\nu} = \mu||\psi^*_{b\alpha}\psi_{b\beta}||$, where $\alpha, \beta = e, x$ and $\mu \equiv \sqrt{2}G_{\rm F}n_\nu(1 - \boldsymbol{v}_b \cdot \boldsymbol{v}_e)$ is the potential due to the $\nu\nu$- interactions, $\boldsymbol{v}_e$ and $\boldsymbol{v}_b$ are velocities of the probe and background neutrinos and n_ν is the neutrino density. (In a single angle approximation $\mu = \sqrt{2}G_{\rm F}n_\nu$.)

The key point is that the background should be in the mixed flavor state. For pure state the off-diagonal terms are zero. Therefore flavor evolution can not be triggered by these self-interactions. It should be triggered by some other effect.

Inclusion of the neutrino self-interactions into the evolution equation (9) is straightforward:

$$\partial_t \boldsymbol{P}_\omega = (\omega\boldsymbol{B} + \lambda\boldsymbol{L} + \mu\boldsymbol{D}) \times \boldsymbol{P}_\omega\,. \tag{28}$$

The new term $\mu\boldsymbol{D}$ describes effect of ν–ν scattering and its structure is rather transparent:

$$\boldsymbol{D} \equiv \int\limits_{-\infty}^{\infty} d\omega\, {\rm Sign}(\omega)\boldsymbol{P}_\omega\,, \tag{29}$$

is the collective neutrino vector, the ${\rm Sign}(\omega)$ reflects that neutrino and antineutrino contribute with opposite signs, thus $\boldsymbol{D}$ represents the net lepton number.

Unless there is an MSW resonance in the dense-neutrino region, one can eliminate $\lambda \boldsymbol{L}$ from Eq. (30) by going into a rotating frame [32,33]. The EOM then takes on the simple form

$$\partial_t \boldsymbol{P}_\omega \approx (\omega \boldsymbol{B} + \mu \boldsymbol{D}) \times \boldsymbol{P}_\omega \,. \tag{30}$$

Performing integration of this equation over ω with $\mathrm{Sign}(\omega)$, one gets the equation for $\boldsymbol{D}$:

$$\partial_t \boldsymbol{D} = \boldsymbol{B} \times \boldsymbol{M} \,, \qquad \boldsymbol{M} \equiv \int\limits_{-\infty}^{\infty} d\omega \, \omega \, \mathrm{Sign}(\omega) \boldsymbol{P}_\omega \,. \tag{31}$$

Eqs. (30) and (31) compose the complete system of master equations.

One phenomenon — synchronized oscillations [27, 29] — follows from these equations immediately. When μ is large, $\mu \boldsymbol{D} \gg \omega$ (large neutrino density), we obtain equations

$$\partial_t \boldsymbol{P}_\omega \approx \mu \boldsymbol{D} \times \boldsymbol{P}_\omega \,. \tag{32}$$

which does not depend on ω, so that the evolution is the same for all modes and $\boldsymbol{P}_\omega$ remain pinned to each other. Furthermore, according to (31) $\boldsymbol{M} = \omega_{\mathrm{syn}} \boldsymbol{D}$, where ω_{syn} is some effective average frequency which is called the synchronization frequency. Then the equation for $\boldsymbol{D}$ becomes $\partial_t \boldsymbol{D} = \omega_{\mathrm{syn}} \boldsymbol{B} \times \boldsymbol{D}$. In this case the individual vectors precess very quickly around $\boldsymbol{D}$ with the same high frequency $\mu |\boldsymbol{D}|$, whereas the collective vector $\boldsymbol{D}$ precesses around $\boldsymbol{B}$ with much smaller synchronization frequency.

Since $\boldsymbol{B}$ is constant, equation for $\boldsymbol{D}$ shows that $\partial_t (\boldsymbol{D} \cdot \boldsymbol{B}) = 0$ and therefore

$$\boldsymbol{B} \cdot \boldsymbol{D} = \mathrm{const} \,. \tag{33}$$

This picture is simplified: one needs to take into account *e.g.* difference of evolution along different trajectories of neutrinos.

4.2. Spectral splits

Collective effects lead to rather complicated dynamics: some phenomena have transient character: show up only in the restricted space region. The other lead to observable effects. One of such phenomena is *spectral split* [35, 36] or swap (according to terminology in [37]).

An example of split is shown in Fig. 4 where the original thermal ν_e and $\bar{\nu}_e$ flux spectra are taken with equal average energies of 15 MeV but an overall $\bar{\nu}_e$ flux that is only 70% of the ν_e flux. The smaller fluxes of the other species ν_μ, ν_τ, $\bar{\nu}_\mu$ and $\bar{\nu}_\tau$ are completely ignored. The two-flavor oscillations

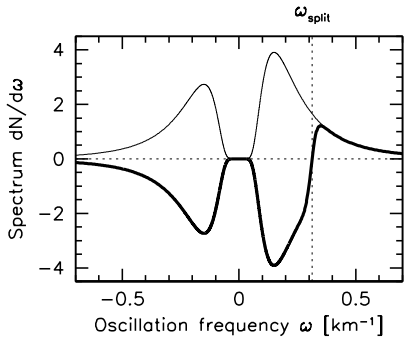

Fig. 4. Neutrino frequency spectra at the neutrino sphere (thin lines) and beyond the dense-neutrino region (thick lines) for the schematic SN neutrino model described in the text. Here $\omega < 0$ is for antineutrinos, $\omega > 0$ for neutrinos.

between ν_e and another flavor ν_x are driven by the atmospheric mass squared difference $\Delta m^2 = (2\text{–}3)\times 10^{-3}$ eV^2 and the small 1–3 mixing angle. In Fig. 4 from [36] the z–components of the usual two-flavor polarization vectors are shown, where "up" denotes the e–flavor and "down" the x–flavor. According to the figure all modes with $\omega < \omega_{\rm split}$ change flavor, whereas the ones with $\omega < \omega_{\rm split}$ stay in their original flavor.

The spectral split is a consequence of

1. existence of special "co-rotating" adiabatic frame in the flavor space which rotates around $\boldsymbol{B}$ with certain frequency $\omega_{\rm c}$ (it rotates together with vector $\boldsymbol{D}$);

2. change (decrease) of the neutrino density: $\mu \to 0$;

3. adiabatic evolution of the neutrino ensemble in the adiabatic frame.

The split frequency is given by the limit $\omega_{\rm split} = \omega_{\rm c}(\mu \to 0)$.

Let us provide with some schematic explanation of the split phenomenon following [36]. According to (30) an "individual Hamiltonian" for a given mode is

$$\boldsymbol{H}_\omega = \omega \boldsymbol{B} + \mu \boldsymbol{D}\,. \tag{34}$$

$\boldsymbol{D}$ and therefore $\boldsymbol{H}_\omega$ precesses around $\boldsymbol{B}$ with the synchronization frequency. In turn, the polarization vectors precess around the Hamiltonians.

One can simplify description performing transition to new reference frame in which motion of the Hamiltonians is slow and therefore the adiabatic approximation can be used. We call this frame the adiabatic frame. Indeed, according to (34) the single-mode Hamiltonians $\boldsymbol{H}_\omega$ always lie in a plane spanned by the vectors $\boldsymbol{B}$ and $\boldsymbol{D}$. Relative to the laboratory frame, this common or co-rotating plane moves around $\boldsymbol{B}$ with the instantaneous co-rotating frequency $\omega_{\rm c}$. To exclude fast rotation of $\boldsymbol{D}$ let us transform to this

"co-rotating" frame. The Hamiltonians in the co-rotating frame are

$$\boldsymbol{H}_\omega = (\omega - \omega_{\rm c})\,\boldsymbol{B} + \mu \boldsymbol{D}\,. \tag{35}$$

If μ changes slowly enough, the motion in the "co-rotating" frame can be adiabatic.

Suppose in initial moment μ is very large and all neutrinos are produced in the same flavor. Then all $\boldsymbol{H}_\omega$ and $\boldsymbol{P}_\omega$ are aligned with the same direction of $\boldsymbol{D}$. Adiabatic solution means that $\boldsymbol{P}_\omega$ follow their Hamiltonians $\boldsymbol{H}_\omega(\mu)$ in the course of evolution. Consequently, the adiabatic solution for our initial condition is given by

$$\boldsymbol{P}_\omega(\mu) = \hat{\boldsymbol{H}}_\omega(\mu)\, P_\omega\,, \tag{36}$$

where $P_\omega = |\boldsymbol{P}_\omega|$ and $\hat{\boldsymbol{H}}_\omega \equiv \boldsymbol{H}_\omega/|\boldsymbol{H}_\omega|$ is a unit vector in the direction of the Hamiltonian. According to Eq. (36), all $\boldsymbol{P}_\omega$ being confined to the co-rotating plane evolve in this frame according to the change of μ.

Now it is straightforward to write final result of evolution. According to Eq. (35), in the limit $\mu \to 0$

$$\boldsymbol{H}_\omega \to (\omega - \omega_{\rm c})\,\boldsymbol{B}, \tag{37}$$

where $\omega_{\rm split} = \omega_{\rm c}(\mu \to 0)$. Therefore, in the case of complete adiabaticity all polarization vectors with $\omega > \omega_{\rm c}$ will be aligned with $\boldsymbol{B}$, whereas all polarization vectors with $\omega < \omega_{\rm c}$ will be anti-aligned with $\boldsymbol{B}$. That is, they will be transformed to the opposite flavors.

In what follows we illustrate the spectral splits using two examples of box-like spectra.

1. The case of only neutrinos with flat distribution in the interval of frequencies $0 \le \omega \le 2\omega_0$ is shown in Fig. 5. Deviation from the sharp split (dotted line) is due to the adiabaticity violation for the modes with frequencies close to $\omega_{\rm c}$. In Fig. 6 we show the spatial evolution of different

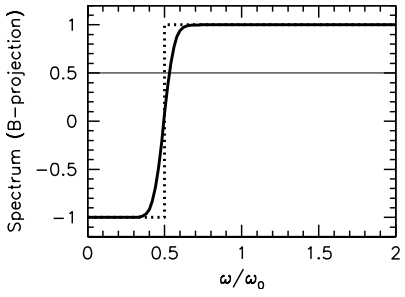

Fig. 5. Initial (thin line) and final (thick line) neutrino spectra. Dotted: fully adiabatic. Solid: numerical example.

modes. Spectrum of frequencies split into two parts. Lines which correspond to one part approach $+1$, others approach -1. The split occurs when μ becomes comparable with ω_0-typical frequency of the spectrum.

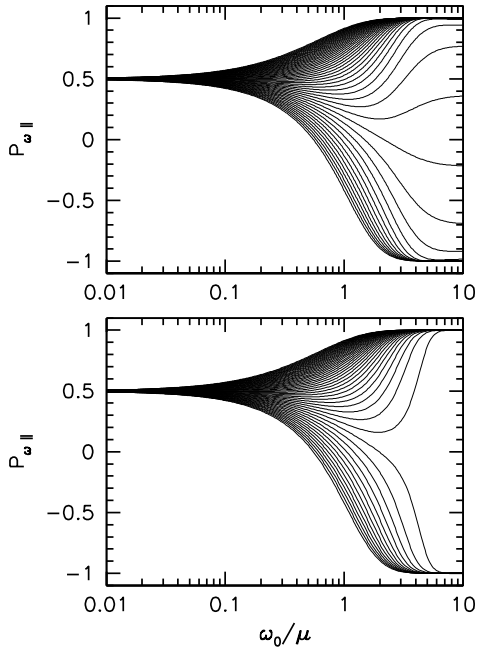

Fig. 6. Evolution of 51 equally spaced modes. Top: numerical solution; Bottom: adiabatic solution.

In Figs. 7 and 8 we show the split in the spectrum which contains both neutrinos and antineutrinos.

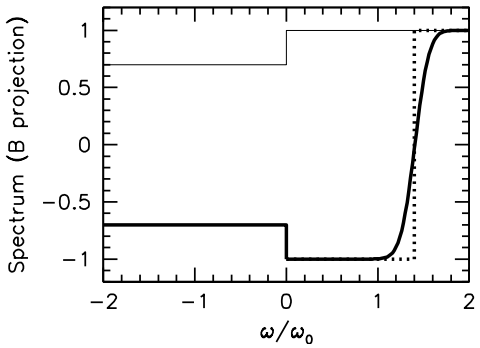

Fig. 7. Neutrino spectra for an initial box spectrum with 70% antineutrinos and $\sin 2\theta_{\rm eff}^{\infty} = 0.05$. Negative frequencies correspond to antineutrinos. Thin line: initial. Thick dotted: final adiabatic. Thick solid: numerical example.

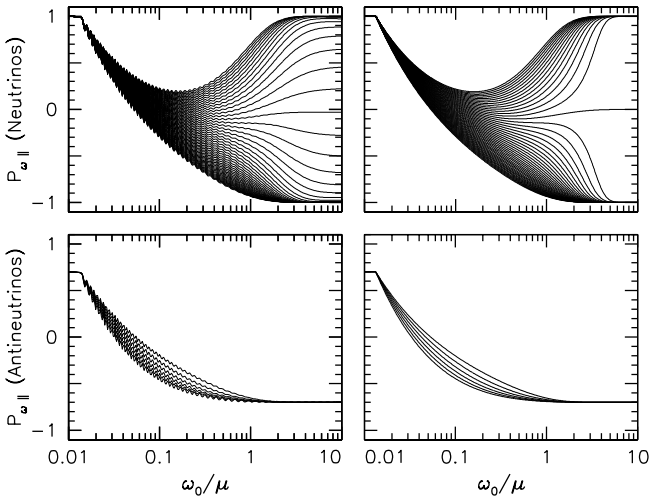

Fig. 8. $P_{\omega B}(\mu)$ for individual modes for the case of neutrinos plus antineutrinos. Left: numerical solution; for $\sin 2\theta^{\infty}_{\rm eff} = 0.05$. Right: adiabatic solution for $\sin 2\theta^{\infty}_{\rm eff} = 0$. In each case neutrinos with 51 modes (top) and antineutrinos with 6 modes (bottom).

5. Toward the underlying physics

The present situation can be characterized in the following way: *(i)* Physics behind neutrino mass and mixing is not identified yet. *(ii)* Certainly this is something beyond the standard model. *(iii)* Data show both order and some degree of randomness and therefore no simple "one-step" explanation is expected. *(iv)* Furthermore, different pieces of data testify for different underlying physics. Below I will present some illustrations of these statements.

6. Analyzing results. Quarks and leptons

Three different possibilities for the lepton mixing have been explored recently: the tri-bimaximal mixing, the quark–lepton complementarity and quark–lepton universality. They have different implications for fundamental physics, and in particular, for the quark–lepton connections.

6.1. Tri-bimaximal mixing

The tri-bimaximal mixing (TBM) matrix is defined as [38]:

$$U_{\rm tbm} \equiv U^{\rm m}_{23} U_{12}(\theta_{12}) = \frac{1}{\sqrt{6}} \begin{pmatrix} 2 & \sqrt{2} & 0 \\ -1 & \sqrt{2} & \sqrt{3} \\ 1 & -\sqrt{2} & \sqrt{3} \end{pmatrix}, \qquad (38)$$

where $U_{23}^{\rm m}$ is the maximal ($\pi/4$) rotation in the 2–3 plane and $\sin^2\theta_{12} = 1/3$; the 1–3 mixing angle is exactly zero. TBM agrees within 1σ with the present experimental results. It is not clear whether it should be considered as just an "organizing" structure, or as something which has deep physical meaning.

If not accidental, it implies possibly some special symmetry in the lepton sector. The following representation of TBM gives a hint of underlying physics

$$U_{\rm tbm} = U_{\rm mag} U_{13}(\pi/4)\,, \tag{39}$$

where $U_{\rm mag}$ is the magic matrix [38]. "Tri-bimaximal equals magic times 1–3 maximal." Majority of models proposed so far are based on the discrete symmetry group A_4 [39]. Other possibilities explored in this connection include models based on the groups T', D_4, S_4, $\Delta(3n^2)$.

Generic features of the proposed models are extended Higgs sector, requirement of particular vacuum alignment which implies further complications of models, auxiliary symmetries. In these models there is no relation between masses and mixing. Mass spectrum is not predicted. Extension to the quark sector is problematic; in the most advanced models it is achieved by different flavor properties of quarks and leptons and different ways of breaking of the flavor symmetry in the quark and lepton sector. This makes further unification of quarks and leptons (or GUT) even more difficult. TBM may indicate that quarks and leptons are fundamentally different.

TBM can be considered as a kind of zero order structure with certain corrections. (In any case it is not RG invariant.) Corrections can lead to correlated non-zero 1–3 mixing and deviation of 2–3 mixing from maximal. Usually it is difficult to get large deviation form the 2–3 mixing in specific models constructed to explain TBM. This can be used for future experimental tests.

6.2. Quark–lepton complementarity

The quark–lepton complementarity (QLC) [40] is another possible guideline which has completely different implications. It is based on observation that $\theta_{12}^l + \theta_{12}^q \approx \pi/4$ and $\theta_{23}^l + \theta_{23}^q \approx \pi/4$. For several reasons it is difficult to expect exact QLC relations, still qualitatively one sees certain correlations

- the 2–3 leptonic mixing is close to the maximal one because the 2–3 quark mixing is small;
- the 1–2 leptonic mixing deviates from the maximal one substantially because the 1–2 mixing (Cabibbo angle) is relatively large.

A general scheme of QLC is

$$\text{lepton mixing} = \text{bimaximal mixing} - \text{CKM}\,, \tag{40}$$

where $U_{\rm CKM}$ is the quark mixing matrix and $U_{\rm bm}$ is the bimaximal mixing matrix:

$$U_{\rm bm} \equiv U_{23}^{\rm m} U_{12}^{\rm m} = \frac{1}{2} \begin{pmatrix} \sqrt{2} & \sqrt{2} & 0 \\ -1 & 1 & \sqrt{2} \\ 1 & -1 & \sqrt{2} \end{pmatrix} . \tag{41}$$

Possible implications of the QLC relations are the following:

1. quark–lepton symmetry or unification: apparently leptons should know about quark mixing; alternatively, the information about quark mixing can be communicated to the lepton sector via the horizontal (flavor) symmetry;

2. existence of structure in the lepton sector which produces the bimaximal mixing; it can be the seesaw itself with certain properties of the RH neutrino mass matrix.

The way it can work is the following. In the lowest order the mixing matrices of quarks and leptons can be

$$V_{\rm quarks} = I\,, \qquad U_{\rm lepton} = U_{\rm bm}\,. \tag{42}$$

Then corrections, having the same origin, generate the quark mixing and simultaneously, the deviation of the lepton mixing from maximal value.

There are two realizations of QLC determined by the order of the bimaximal and CKM rotations:

$$U_{\rm PMNS} = U_{\rm bm} U_{\rm CKM}^{\dagger}\,, \tag{43}$$

denoted QLC$_l$ and

$$U_{\rm PMNS} = U_{\rm CKM} U_{\rm bm} \tag{44}$$

called QLC$_\nu$. Since the neutrino states appear from the left and charge lepton states from the right side of $U_{\rm PMNS}$ one can assume that in the case of QLC$_l$ the bimaximal mixing comes from the charged leptons, whereas in QLC$_\nu$ — from neutrinos. In the latter case the seesaw mechanism can be the origin of the bimaximal mixing.

The two versions differ by predictions of the 1–2 mixing angle θ_{12}:

$$\text{QLC}_\nu\colon\ 35.4^\circ\,, \qquad \text{TBM}\colon\ 35.2^\circ\,, \qquad \text{QLC}_l\colon\ \pi/4 - \theta_{\rm C} = 32.2^\circ\,, \tag{45}$$

as well as by the 1–3 mixing angle θ_{13}:

$$\text{QLC}_\nu\colon\ 9^\circ\,, \qquad \text{TBM}\colon\ 0\,, \qquad \text{QLC}_l\colon\ 1.5^\circ\,. \tag{46}$$

Notice that $\theta_{12}(\text{QLC}_\nu) \approx \theta_{12}(\text{TBM})$. Both QLC realizations agree with the present data within 1σ. Clearly, combination of future precise measurements of these angles will allow us to disentangle the three possibilities. Recall, all these predictions can be changed due to appearance of the CP-violation phases and by the RGE effects.

6.3. Real or accidental?

There is a number of observations which can testify for certain symmetry or particular relations: maximal 2–3 mixing, tri-bimaximal mixing, small (zero) 1–3 mixing, Koide relation between masses of charged leptons which is probably in the same line as TBM, the QLC relations. Are these features accidental? We can say that *e.g.* some value of mixing angle is accidental if it is a combination (interplay) of two (or more) independent contributions. If some value or relation is immediate consequence of symmetry, we conclude that they are not accidental, that is, real.

Another important question: Are smallness of neutrino mass and the observed pattern of mixing related? As some models show, mixing pattern can be immediate consequence of symmetry for arbitrary values of masses. In this sense masses and mixing decouple.

6.4. Quark–lepton universality

One consider an approach which does not rely on any specific symmetry in the lepton sector. Mass (Yukawa coupling) matrices in the quark and lepton sectors may have no fundamental distinction. Whole difference is related to the seesaw mechanism of neutrino mass generation which explains simultaneously the smallness of neutrino mass and large lepton mixing.

It has been shown that universality of the Dirac mass matrices of quarks and leptons can be realized and the difference of observables steams from the Majorana mass matrix of the RH neutrinos.

7. Standard neutrino scenario

7.1. Standard scenario

"Standard neutrino scenario" — new paradigm in neutrino physics can be formulated in the following way:

- there are only 3 types of light neutrinos (three flavor and three mass states);
- neutrino interactions are described by the standard electroweak model;
- masses and mixing have pure vacuum origin: they are generated at the electroweak and probably higher energy scales. These are "hard" masses: The VEV's involved are large or, if small, induced by other large VEV's, as in the case of seesaw type-II.

The main goal of the present phenomenological programs is to test these statements and search for "physics beyond". On the theoretical side, the most appealing line of understanding neutrino mass and mixing includes *(i)* the see-saw mechanism; *(ii)* quark–lepton unification; *(iii)* SO(10) GUT.

Do neutrinos provide an evidence of GUT? Via the seesaw mechanism, the values RH neutrino masses indicate existence of scale which can coincide with the GUT scale, $M_{\rm GUT}$, (the scale of possible unification of three gauge couplings). There are two different realizations of relation of neutrino mass and $M_{\rm GUT}$.

1. In the presence of mixing of three generations, the value of mass of the heaviest RH neutrino can coincide with the GUT scale

$$M_R \approx M_{\rm GUT} \sim 10^{16}\,{\rm GeV}\,. \tag{47}$$

Notice that due to large lepton mixing the mass of the heaviest neutrino is related to the mass of the lightest light neutrino. Since the RH neutrinos are singlets of the SM gauge groups exact equality (47) or connection may not exist.

2. The scale of RH neutrino masses can be related to $M_{\rm GUT}$ via the Planck scale $M_{\rm Pl}$:

$$M_R \approx \frac{M_{\rm GUT}^2}{M_{\rm Pl}} \sim 10^{14}\,{\rm GeV}\,. \tag{48}$$

This relation is realized, *e.g.*, in the double seesaw scenario [42].

Other way around: GUT's provide with all the ingredients which are necessary for the seesaw mechanism: *(i)* existence of the RH neutrinos; *(ii)* large mass scale; *(iii)* lepton number violation. They give relations between masses of leptons and quarks, *e.g.* $m_b = m_\tau$, and in general, "sum rules" which connect masses and mixings, for instance, the $b-\tau$ unification can be connected to the large lepton mixing [43]. However (with few exceptions), GUT's do not explain the flavor structure: *(i)* number of generations, *(ii)* mass hierarchies, *(iii)* mixing patterns. It is assumed that certain flavor symmetry is responsible for the observed flavor structures. Analysis shows that it is not trivial to reconcile (A) the existing data on mass and mixing, (B) GUT, and (C) flavor symmetries. From other perspective: data and flavor symmetries prevent from GUT. To explain data with flavor symmetries the quarks and leptons, the RH components of charged leptons and neutrinos should have different flavor properties (transform differently under flavor group). This prevents their unification. The flavor symmetry should be broken in rather complicated way.

7.2. Bottom–up

Leptons and quarks have similar gauge structure, there is clear correspondence or symmetry between the quark and lepton sectors. At the same time, quarks and leptons have very different mass and mixing pattern. This testifies for existence of additional structure in the lepton sector which produces these differences. Plausible answer is that the see-saw with its Majorana

mass matrix of RH neutrinos (which has no analogy in the quark sector) plays the role of this additional structure. It is the seesaw that enhances the lepton mixing. Furthermore, the seesaw may generate some symmetry at the effective level of the light neutrino mass matrix, after decoupling of heavy neutrinos. Such a symmetry may not exist at the fundamental level as symmetry of the Lagrangian, where both the LH and RH neutrino components are present. We can call this the *seesaw symmetry*. Is the seesaw enough to explain data? Is something missed?

There are two different views on the problem: from the bottom and from the top. The data do not show simple relations between masses and mixings (although there were numerous attempts to find some universal formulas, examples being $\tan 2\theta_{\rm c} = 1/2$, golden ratio, Koide relation *etc.*); they can not be described in terms of few (1–2) parameters. It seems there is no simple "one-step" explanation. From this point of view data look complicated. Looking from the top we find very rich string theory "offer" which includes GUT, existence of large $\sim O(100)$ number of gauge singlets (SM as well as GUT symmetry group); several U(1) gauge factors; various discrete symmetries, heavy vector-like families of fermions, non-renormalizable operators, selection rules for interactions which cannot be expressed in terms of symmetries at the field theory level; explicit violation of symmetries; incomplete gauge multiplets, *etc.* So, one can wonder how this complicated structure at high energies leads to so simple structure which we observe at low energies? Why the data look simple?

8. Beyond the "standard neutrino scenario"

New physics can be related to

1. new neutrino states,
2. new neutrino interactions,
3. new dynamics in neutrino propagation.

Some examples of this new physics and comments are given below.

8.1. New neutrino states

New neutrino states with mass $m \leq m_Z/2$ should be sterile or almost sterile. If light, they can have direct observable consequences: be produced in various neutrino processes, participate in oscillations, decays, *etc.* New states can also produce indirect effects: modification of the mass matrix of active neutrinos ("invisible mixing"), breaking of universality, appearance of FCNC. Light sterile neutrinos both participate in low energy phenomenology and modify mass matrix of active neutrinos. Depending on values of masses and mixing direct or indirect effects can dominate. Heavy sterile neutrinos decouple producing indirect effects only.

A general picture is that new gauge singlets form a hidden sector with some symmetries which determine their mass spectrum. These singlets can couple (mix) with LH components directly, or/and indirectly via couplings (mixing) with the RH components. Apparently, these singlets can mix with neutrinos only and, therefore, potentially explain different patterns of quarks and leptons. These singlets (on top of the seesaw) can be an additional structure needed to explain observations.

The bounds on mixing of the sterile neutrinos with active neutrinos, θ_S, strongly depend on mass of S, m_S. The bounds follow (moving from smaller to higher values of m_S) from *(i)* the atmospheric neutrino and *(ii)* reactor neutrino studies, *(iii)* cosmology (large scale structure of the Universe, LSS), *(iv)* X-ray spectrum in the Universe, *(v)* CMB, *(vi)* accelerator experiments (production of S in the decay of K-mesons), *(vii)* neutrinoless double beta decay (for the electron neutrino).

The induced due to mixing with sterile neutrino mass of the active neutrino mass equals

$$m_{\rm ind} = m_S \sin^2 \theta_S \,. \tag{49}$$

When $m_S \sin^2 \theta_S \geq 0.025\,\text{eV}$, the induced mass $m_{\rm ind}$ is of the order of dominant mass terms, that is, it can generate the dominant structure of the mass matrix. For $m_S \sin^2 \theta_S \geq 0.003\,\text{eV}$, the induced mass can be responsible for the sub-dominant mass structures. Below $m_S \sin^2 \theta_S \sim 0.001\,\text{eV}$ effect of induced mass on the neutrino mass matrix is negligible. Notice that for all benchmark parameters mentioned above the sterile neutrino is thermalized in the Early Universe.

Large part of the region where S can produce significant effect on the active neutrino mass and mixing is already excluded by the astrophysical and cosmological observations. Still small window near 0.1 eV is allowed. Also in the region $m_S >$ several 100 MeV the influence of active-sterile mixing can be substantial. Unfortunately, it is difficult to test this region. Bound on mixing of S with ν_μ and ν_τ are weaker in some ranges.

8.2. New interactions

One can classify new interactions as

1. Short range interactions due to exchange of heavy particles with masses at the electroweak scale and larger. Examples being new gauge bosons, scalar bosons of extended Higgs sector, SUSY particles, *etc.*

2. Long range interactions due to exchange of new light particles *e.g.* new scalars: majorons, accelerons, cosmons, *etc.* Introduction of these new particles has certain cosmological motivations.

Exchange of light scalar bosons can lead to appearance of effective soft neutrino masses which depend on properties of medium and disappear in vacuum. One example is a very light scalar with mass $m_\phi = (10^{-8}$–$10^{-6})\,\mathrm{eV}$ which appears, *e.g.* in the context of MaVaN scenario [44]. If λ_f are the coupling constants of the scalar with neutrinos and charged fermions $f = e, u, d, \nu$, then exchange of this scalar will generate the neutrino mass

$$m_{\mathrm{soft}} = \frac{\lambda_\nu \lambda_f n_f}{m_\phi^2}\,, \tag{50}$$

where n_f is the density of fermions. The total mass which appears in the evolution equation equals

$$m_{\mathrm{tot}} = m_{\mathrm{vac}} + m_{\mathrm{soft}}\,, \tag{51}$$

where m_{vac} is generated by vacuum — some VEV of the scalar field. The present experimental results give various bounds on the soft component of mass.

8.3. Something completely different

Existence of extra spatial dimensions opens qualitatively new possibility to generate small Dirac masses of neutrinos. The left and the right components of neutrinos can have different localizations in extra dimensions. Value of Yukawa coupling in 4D is then proportional to degree of overlap of the LH and RH component of wave functions or the overlap factor κ. Then neutrino mass in 4D can be written as

$$m_{\mathrm{D}} = \lambda v_{\mathrm{EW}} \xi\,, \tag{52}$$

where $\lambda \sim 1$ and v_{EW} is the electroweak VEV.

Due to the fact that the RH neutrinos have no SM interactions, their localization can be substantially different which leads to strong suppression of masses. This mechanism can be called the overlap suppression.

Let us evaluate the overlap (suppression) factor in different scenarios with extra dimensions.

1. Large flat extra dimensions. The 3D spatial brane is embedded in $(3+\delta)$D bulk [45] of extra dimensions. Extra dimensions have large radii $R_i \gg 1/M_{\mathrm{Pl}}$ which allows one to reduce the fundamental scale of theory down to $M^* \sim 10$–100 TeV [45].

The left handed neutrino is localized on the brane, whereas the right handed component (being a singlet of the gauge group) propagates in the bulk. For one extra D with coordinate y the normalization condition gives a typical value of the wave function $\nu_{\mathrm{R}}(y) \sim 1/\sqrt{R}$. The width of the

brane is of the order of $d \sim 1/M^*$, therefore the overlap factor with the LH component which is localized on the brane equals

$$\xi = d^{1/2}\nu_{\rm R} \sim \frac{1}{\sqrt{M^* R}}\,. \tag{53}$$

For δ extra dimensions we get for the overlap factor $\xi = 1/\sqrt{M^{*\delta} V_\delta}$, where V_δ is the volume of extra dimensions.

2. Warped extra dimensions. Two branes, the visible and "hidden", are localized in different points of extra dimension with non-factorizable metric [46]. The wave function of the RH neutrino $\nu_{\rm R}(\phi)$ is centered on the hidden brane, whereas the LH one — on the visible brane. Due to warp geometry $\nu_{\rm R}$ exponentially decreases from the hidden to the observable brane. The overlap factor is given by the value of $\nu_{\rm R}$ on the visible brane:

$$\xi = \nu_{\rm R}^{\rm (vis)} \sim \epsilon^{\nu - 1/2}\,, \qquad \epsilon = e^{-k r_c \pi} = \frac{v_{\rm EW}}{M_{\rm Pl}}\,. \tag{54}$$

Here $M_{\rm Pl}$ is the Planck scale, r_c is the radius of extra dimension, $k \sim M_{\rm Pl}$ is the curvature parameter. In (54) $\nu \equiv m/k$ and $m \sim M_{\rm Pl}$ is the Dirac mass in 5D. For $\nu = 1.1$–1.6 we obtain the mass in the required range.

3. The LH and RH neutrino wave functions can be localized differently on the same "fat" brane [47]. One possibility is to localize $\nu_{\rm L}$ and $\nu_{\rm R}$ in different places of the brane; or the RH neutrino can be localized in the narrow region of the fat brane, whereas the LH neutrino wave function spans whole the brane.

9. Conclusion

Developments during last 10 years were the real breakthrough in the field:

- — discovery of neutrino mass,
- — determination of the dominant structure of lepton mixing, discovery of two large mixing angles,
- — establishing strong difference of the quark and lepton mixing patterns on the top of smallness of neutrino mass.

With these discoveries, it seems, we are touching something really new. However, in spite of plenty of proposed models and approaches, no unique and convincing scenario of the underlying physics beyond the standard model has been found. Nevertheless, one may start to think about applications and developments of neutrino technologies for geophysics, the Earth tomography, search for oil and minerals, control of atomic reactors, *etc.*

What is next? New measurements will allow us hopefully to establish type of neutrino mass spectrum (quasi-degenerate, hierarchical); type of mass hierarchy, nature of neutrino and neutrino mass. Sooner or latter we will measure the 1–3 mixing, deviation of 2–3 mixing from maximal, and CP-phases. We will test predictions of particular models.

All this may discriminate various possibilities but not lead to final answer (identification of physics behind neutrino masses and mixing). LHC and other non-neutrino experiments may check low scale mechanisms of neutrino mass generation as well as test a context (*e.g.* SUSY).

From theoretical side one can find two points of view: *(i)* There is nothing fundamental behind values of neutrino mass and mixing: the observed values are accidental interplay of several (many) essentially unrelated factors, result of some complicated evolution (*á la* the planetary system). *(ii)* The observed structures will have explanations at the field theory level in terms of certain (broken) symmetries, properties of vacuum, *etc.* The hope is that neutrinos will uncover something simple and illuminating which will shed some light on fermion masses problem and allow us to identify new physics beyond the standard model.

REFERENCES

[1] B. Pontecorvo, *Zh. Eksp. Theor. Fiz.* **33**, 549 (1957); **34**, 247 (1958).

[2] Z. Maki, M. Nakagawa, S. Sakata, *Prog. Theor. Phys.* **28**, 870 (1962).

[3] J. Conrad, talk at this Meeting not included in the proceedings.

[4] H.V. Klapdor-Kleingrothaus, *et al., Phys. Lett.* **B586**, 198 (2004); H.V. Klapdor-Kleingrothaus, I. Krivosheina, *Mod. Phys. Lett.* **A21**, 1547 (2006).

[5] A. Goobar, S. Hannestad, E. Mortsell, H. Tu, `astro-ph/0602155`.

[6] U. Seljak, A. Slosar, P. McDonald, `arXiv:astro-ph/0604335`.

[7] G.L. Fogli *et al.*, `arXiv:0805.2517 [hep-ph]`.

[8] [MiniBooNE Collaboration], `arXive:0704.1500`.

[9] A. Aguilar *et al.* [LSND Collaboration], *Phys. Rev.* **D64**, 112007 (2001).

[10] B. Pontecorvo, *Zh. Eksp. Theor. Fiz.* **53**, 1771 (1967); [*Sov. Phys. JETP* **26**, 984 (1968)]; V.N. Gribov, B. Pontecorvo, *Phys. Lett.* **B28**, 493 (1969).

[11] L. Wolfenstein, *Phys. Rev.* **D17**, (1978) 2369; in *Neutrino-78*, Purdue Univ. **C3**, (1978); *Phys. Rev.* **D20**, 2634 (1979).

[12] S.P. Mikheyev, A.Yu. Smirnov, *Sov. J. Nucl. Phys.* **42**, 913 (1985); *Nuovo Cim.* **C9**, 17 (1986); S.P. Mikheev, A.Yu. Smirnov, *Sov. Phys. JETP* **64**, 4 (1986).

[13] A.Yu. Smirnov, `hep-ph/0702061`.

[14] V.K. Ermilova, V.A. Tsarev, V.A. Chechin, *Kr. Soob. Fiz.* **5**, 26 (1986); Short Notices of the Lebedev Institute; E.K. Akhmedov, *Sov. J. Nucl. Phys.* **47**, 301 (1988).

[15] E.K. Akhmedov, *Nucl. Phys.* **B538**, 25 (1999).

[16] S.T. Petcov, *Phys. Lett.* **B434**, 321 (1998); M.V. Chizhov, M. Maris, S.T. Petcov, arXiv:hep-ph/9810501; M.V. Chizhov, S.T. Petcov, *Phys. Rev.* **D63**, 073003 (2001).

[17] E.K. Akhmedov, M. Maltoni, A.Y. Smirnov, *J. High Energy Phys.* **05**, 077 (2007) [hep-ph/0612285].

[18] E.K. Akhmedov, M. Maltoni, A.Y. Smirnov, arXiv:0804.1466 [hep-ph].

[19] P. Huber, W. Winter, *Phys. Rev.* **D68**, 037301 (2003).

[20] A.Yu. Smirnov, hep-ph/0610198.

[21] Y. Suzuki *et al.* [TITAND Working Group], arXiv:hep-ex/0110005;
Y. Suzuki, Prepared for 3rd International Workshop on NO-VE: Neutrino Oscillations in Venice: 50 Years after the Neutrino Experimental Discovery, Venice, Italy, 7–10 Feb. 2006.

[22] A.S. Dighe, A.Yu. Smirnov, *Phys. Rev.* **D62**, 033007 (2000); C. Lunardini, A.Yu. Smirnov, *JCAP* **0306**, 009 (2003).

[23] H. Minakata, H. Nunokawa, *Phys. Lett.* **B504**, 301 (2001).

[24] V. Barger, D. Marfatia, B.P. Wood, *Phys. Lett.* **B532**, 19 (2002).

[25] K. Takahashi, K. Sato, A. Burrows, T.A. Thompson, *Phys. Rev.* **D68**, (2003) 113009.

[26] J.T. Pantaleone, *Phys. Lett.* **B287**, 128 (1992); J.T. Pantaleone, *Phys. Lett.* **B342**, 250 (1995).

[27] S. Samuel, *Phys. Rev.* **D48**, 1462 (1993).

[28] S. Samuel, *Phys. Rev.* **D53**, 5382 (1996) [hep-ph/9604341].

[29] S. Pastor, G. Raffelt, *Phys. Rev. Lett.* **89**, 191101 (2002) [astro-ph/0207281];

[30] A. Friedland, C. Lunardini, *Phys. Rev.* **D68**, 013007 (2003).

[31] R.F. Sawyer, *Phys. Rev.* **D72**, 045003 (2005).

[32] H. Duan, G.M. Fuller, Y.Z. Qian, *Phys. Rev.* **D74**, 123004 (2006) [astro-ph/0511275].

[33] S. Hannestad, G.G. Raffelt, G. Sigl, Y.Y.Y. Wong, *Phys. Rev.* **D74**, 105010 (2006).

[34] G.M. Fuller, Y.Z. Qian, *Phys. Rev.* **D73**, 023004 (2006).

[35] H. Duan, G.M. Fuller, J. Carlson, Y.Z. Qian, *Phys. Rev.* **D74**, 105014 (2006) [astro-ph/0606616]; H. Duan, G.M. Fuller, J. Carlson, Y.Z. Qian, *Phys. Rev.* **D75**, 125005 (2007) [astro-ph/0703776].

[36] G.G. Raffelt, A.Yu. Smirnov, *Phys. Rev.* **D76**, 081301 (2007); *Phys. Rev.* **D76**, 125008 (2007).

[37] H. Duan, G.M. Fuller, J. Carlson, Y.Q. Zhong, astro-ph/0707.0290.

[38] L. Wolfenstein, *Phys. Rev.* **D18**, 958 (1978); P.F. Harrison, D.H. Perkins, W.G. Scott, *Phys. Lett.* **B458**, 79 (1999); *Phys. Lett.* **B530**, 167 (2002).

[39] E. Ma, *Mod. Phys. Lett.* **A17**, 2361 (2002); G. Rajasekaran, *Phys. Rev.* **D64**, 113012 (2001); K.S. Babu, E. Ma, J.W.F. Valle, *Phys. Lett.* **B552**, 207 (2003).

[40] A.Yu. Smirnov, `hep-ph/0402264`; M. Raidal, *Phys. Rev. Lett.* **93**, 161801 (2004); H. Minakata, A.Yu. Smirnov, *Phys. Rev.* **D70**, 073009 (2004).

[41] M.A. Schmidt, A.Y. Smirnov, *Phys. Rev.* **D74**, 113003 (2006) [`arXiv:hep-ph/0607232`].

[42] R.N. Mohapatra, *Phys. Rev. Lett.* **56**, 561 (1986); R.N. Mohapatra, J.W.F. Valle, *Phys. Rev.* **D34**, 1642 (1986).

[43] B. Bajc, G. Senjanovic, F. Vissani, *Phys. Rev. Lett.* **90**, 051802 (2003).

[44] P.Q. Hung, `hep-ph/0010126`; Peihong Gu, Xiulian Wang, Xinmin Zhang, *Phys. Rev.* **D68**, 087301 (2003); R. Fardon, A.E. Nelson, N. Weiner, *JCAP* **0410**, 005 (2004) [`hep-ph/0507235`]; D.B. Kaplan, A.E. Nelson, N. Weiner, *Phys. Rev. Lett.* **93**, 091801 (2004).

[45] N. Arkani-Hamed, S. Dimopoulos, G.R. Dvali, J. March-Russell, *Phys. Rev.* **D65**, 02432 (2002); K.R. Dienes, E. Dudas, T. Ghergetta, *Nucl. Phys.* **B557**, 25 (1999).

[46] Y. Grossman, M. Neubert, *Phys. Lett.* **B474**, 361 (2000).

[47] N. Arkani-Hamed, M. Schmaltz, *Phys. Rev.* **D61**, 033005 (2000).